ELSEVIER

Biochimica et Biophysica Acta 1282 (1996) 76–84

BBA Biochimica et Biophysica Acta

Membrane changes associated with the temperature-sensitive P85$^{gag\text{-}mos}$-dependent transformation of rat kidney cells as determined by dielectrophoresis and electrorotation

Ying Huang, Xiao-Bo Wang, Frederick F. Becker, Peter R.C. Gascoyne *

Department of Molecular Pathology, University of Texas, MD Anderson Cancer Center, 1515 Holcombe Boulevard, Houston, TX 77030, USA

Received 28 November 1995; accepted 14 February 1996

Abstract

Conventional dielectrophoresis (cDEP) and electrorotation (ROT) measurements have been used to determine the dielectric properties of a clone of normal rat kidney cells, designated 6m2, that exhibits a transformed phenotype at 33°C and a non-transformed phenotype at 39°C. cDEP measurements of the crossover frequencies at which individual 6m2 cells experienced zero cDEP force performed as a function of the conductivity of the suspension medium revealed that, in response to a temperature shift from 33°C to 39°C for 24 h, the mean specific cell membrane capacitance and conductance fell significantly ($P < 0.01$) from 42.3 ($\pm$1.3) to 30.3 ($\pm$2.9) mF/m^2 and 743 ($\pm$422) to 567 ($\pm$326) S/m^2, respectively. ROT analyses demonstrated a similar reduction for the membrane capacitance from 37.2 ($\pm$7.3) to 27.4 ($\pm$6.1) mF/m^2, and also showed that accompanying changes in the mean internal electrical conductivity and dielectric permittivity of the cells were insignificant. Scanning electron microscopy was used to examine the surface morphology of the cells and, in agreement with our previous reports for leukemia cells, the observed membrane capacitance values correlated closely with the morphological complexity of the cell membrane surface. The observed changes in the membrane dielectric properties are discussed in terms of their biological significance and their relationship to previously-detected changes in cell surface charge.

Keywords: Dielectrophoresis; Electrorotation; Cell dielectric property; Membrane capacitance; Membrane conductance

1. Introduction

Recent conventional dielectrophoresis (cDEP) and electrorotation (ROT) measurements have revealed that significant differences exist in the dielectric properties of different types of cells and of cells in different physiological states [1–16]. For example, the average specific plasma membrane capacitance for human breast cancer cells was found to be 26 mF/m^2, more than twice of that for human T-lymphocytes (11 mF/m^2) [15]. The average membrane capacitance fell by 15% for murine erythroleukemia DS19 cells following differentiation treatment [14], while by contrast it increased from 10 to 13 mF/m^2 for murine lymphocytes following 72 h of mitogenic stimulation [6]. Significant changes in dielectric parameters also occurred when yeast cells responded to environmental toxins [1], when rabbit oocytes were fertilized [4], and when human platelets were activated [16]. These observations demonstrate that cell dielectric characteristics are closely associated with biological function and collectively constitute a physical component of cell phenotype. This dielectric phenotype not only provides a new criterion for the classification of cells but also can be exploited for cell manipulation and separation through the electric field-dependent phenomenon of dielectrophoresis [15,17–20].

Over the last several years our laboratory has been investigating the relationship between the dielectric phenotype and the transformation status of cancer cells using cDEP and ROT measurements. We discovered large changes in the capacitive characteristics of the plasma membranes of both DS19 murine erythroleukemia [12,14,17] and HL60 human leukemia cells following chemically-induced differentiation. Furthermore, we were able to explain these changes in terms of alterations in plasma membrane morphology [14]. In this work we extend those cDEP and ROT studies to the 6m2 cell line, a clone of normal rat kidney cells infected with a tempera-

* Corresponding author. Fax: +1 (713) 7925940.

PII S0005-2736(96)00047-8

ture-sensitive mutant of Moloney sarcoma virus. This line exhibits a transformed phenotype at a permissive temperature of 33°C but a normal phenotype at the nonpermissive temperature of 39°C. Several biophysical studies have been reported previously for 6m2 cells as their phenotype is manipulated by altering the temperature, including measurements of cell transmembrane potentials by the potential-sensitive fluorescent dye diS-C_3-(5) [21] and of surface fixed charges by electrophoresis [22]. Scanning electron microscopy has also been used to characterize cell surface morphology at both permissive (33°C) and nonpermissive temperature (39°C) and as a function of potassium concentration in the growth medium [23].

In this paper the dielectric properties of 6m2 cells at 33°C and 39°C are determined by both cDEP and ROT measurements. cDEP measurements were made by determination of so-called crossover frequencies at which cells experienced zero cDEP force and exhibited no movement. Data were obtained for many individual cells as a function of the suspension conductivity [7,12]. ROT frequency spectra in the range 10 kHz to 100 MHz were also measured for individual cells. Dielectric parameters of the cell membrane and cytoplasm were derived by fitting the single shell dielectric model to the experimental data [7,12]. Both the cDEP and ROT measurements revealed that the mean specific membrane capacitance fell by about 26% when cells were shifted from the permissive temperature (33°C) to the non-permissive temperature (39°C). In agreement with earlier results for HL60 and DS19 cells [14] and other cells [11,24], we conclude that this observed capacitance change arose from modification of the cell surface morphology. Scanning electron microscopy supported this conclusion. The physical significance of the membrane morphology and conductance and of the other parameters are discussed.

2. Materials and methods

2.1. Cells

Transformed 6m2 cells, originally isolated by Blair et al. [25,26], were grown at the permissive temperature of 33°C in McCoy's 5A medium supplemented with 10% fetal bovine serum under standard conditions. Cells of a non-transformed phenotype were produced by shifting cultures to the non-permissive temperature of 39°C for 24 or 48 h before the experiments. All cells were harvested at ~ 80% confluency by 3 min exposure to 0.2% trypsin in serum-free McCoy's medium. Suspended cells were then kept in a reservoir in the incubator in complete medium at the appropriate temperature (33 or 39°C) and fresh aliquots were removed and diluted with sucrose/dextrose buffer (see later) when needed for each measurement over a period not exceeding 2 h post-harvest.

2.2. cDEP crossover frequency

Cells exhibit motion towards or away from strong electrical field regions under the influence of positive or negative cDEP forces [7,9,12,18,27] in an alternating field of non-uniform strength. The cDEP crossover frequency is defined as that frequency at which cDEP forces change polarity and cells experience zero cDEP force. cDEP experiments were conducted using a chamber consisting of a rubber O-ring (15 × 1 mm) affixed with wax to a glass substrate that supported a gold polynomial electrode array having a tip–tip spacing of 400 μm as described previously [9,14,27]. Sinusoidal signals (3 V rms) were applied to neighboring electrode elements using a BK Precision 3011 Function Generator. For each experiment, 200 μl of freshly diluted cell suspension was pipetted into the O-ring and a cover slip was gently depressed over its center to form a tight seal. 6m2 cells were investigated in 250 mM sucrose/18 mM dextrose suspensions at conductivities of 20, 35, 45, 56 and 70 mS/m for both 33°C and 39°C samples. After introduction of a cell suspension, motion of cells towards or away from the electrode edges due to the applied signal was observed. The cDEP crossover frequency was determined for individual cells located ~ 10 μm from an electrode edge by adjusting the frequency of the applied field until cell movement ceased. The crossover frequency for individual cells could be measured to an accuracy better than 3%. Crossover frequencies for at least 15 cells were determined for each experimental condition and the results were analyzed to derive average cell membrane dielectric properties using the procedure explained in the Appendix.

2.3. Electrorotation spectra

Each ROT sample was prepared by diluting 1 part of suspended culture from the reservoir with 21 parts of 250 mM sucrose/18 mM dextrose solution to yield a suspension of conductivity 56 mS/m. Each ROT spectrum over the frequency range 10 kHz to 100 MHz was measured at room temperature (22 ± 0.5°C) in the same chamber used for cDEP experiments and took ~ 20 min to complete. After cells had settled for about 2 min, a 20-kHz voltage was applied to the electrodes for 10 s to move cells into the central region of the electrodes by negative cDEP [9,27]. A rotating field was then established by energizing the 4 polynomial electrode elements with sinusoidal voltages of 0.9 V (rms) in phase quadrature, provided by a specially-built signal generator and supplied via four 50 Ω coaxial cables terminated with 50 Ω resistors between each electrode and signal ground. Cell electrorotation was monitored using a Nikon Diaphot TMD inverted microscope equipped with a Hamamatsu CCD video camera and measured manually using a stopwatch from four separate determinations. Statistical analysis of the timing data for all the cells studied showed that the relative measurement

error is < 4%. ROT measurements were conducted from 100 MHz to 10 kHz at four points per frequency decade, and to minimize the influence of cDEP-induced lateral cell motion [28], only the cells located within 100 μm of the center of the electrode geometry were studied. Cell size was calculated from the direct measurement of cell images on the TV monitors and calibrated against a stage micrometer. ROT spectra were analyzed according to the single shell dielectric model using the minimization method described previously [14,29].

2.4. Scanning electron microscopy (SEM)

The morphologies of 6m2 cells were examined both in suspensions following harvest and in intact monolayer cultures. For cell suspensions, briefly trypsinized 6m2 cells were washed, fixed, rinsed and studied on a Hitachi Model S520 scanning electron microscope as described previously [14]. For cell monolayers, 6m2 cells were cultured to ~ 80% confluency on cover slips at both 33 and 39°C. Cells were then rinsed with balanced salt solution, fixed at 37°C with modified Karnovsky's fixative for at least 30 min, and examined according to the method outlined in Ref. [14].

3. Results

3.1. cDEP crossover frequencies

Crossover frequencies, f_{cross}, for individual 6m2 cells are shown in Fig. 1 as a function of both suspension conductivity and cell radius at 33 and at 39°C. It is clear that f_{cross} increases steadily with increasing conductivity but at different rates for the two cell growth conditions: 33°C cells exhibited a mean increment rate of 700 kHz · m/S over the range of suspension conductivities studied, while those grown at 39°C for 24 h exhibited an increment rate of 1000 kHz · m/S. At each suspension conductivity, the crossover frequencies exhibited no correlation with cell size, and cells from each sample displayed variations of up to 50% in their f_{cross} values, reflecting intrinsic inhomogeneities in the cell electrokinetic responses. Such heterogeneity is to be expected for asynchronous cell cultures of tumorous origin. By analyzing the dependence of f_{cross} on suspension conductivity, cell size, and cell dielectric parameters using the single shell dielectric model (see Appendix), we derived mean specific capacitances of 42.3 ($\pm$1.3) and 30.3 ($\pm$2.9) mF/m^2, and mean specific conductances of 743 ($\pm$422) and 567 ($\pm$326) S/m^2 for 6m2 cells at 33 and 39°C, respectively. Despite the heterogeneities observed in the cell populations at both temperatures, these changes in mean specific capacitance and conductance were significant at a level of $P < 0.01$.

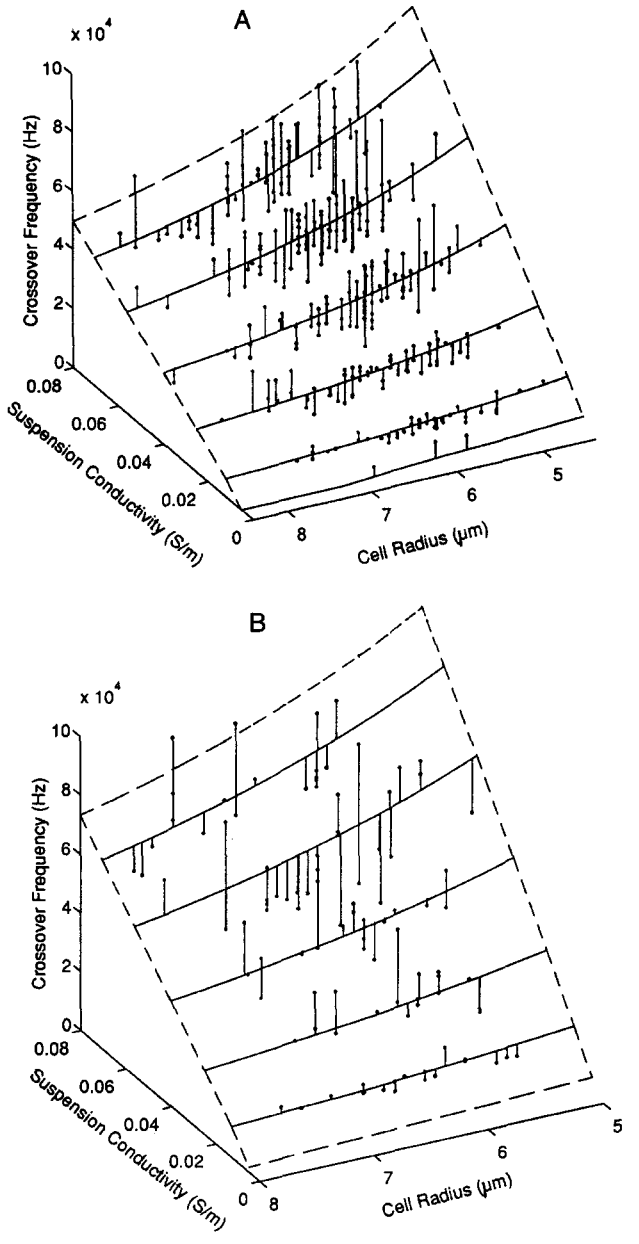

Fig. 1. Dependence of cDEP crossover frequency of individual 6m2 cells grown at 33°C (A) and 39°C for 24 h (B) on cell radius and conductivity of the suspending medium. The surfaces bordered by dashed lines are the best theoretical fits to the experimental data according to Eq. A.4 and Eq. A.5 in the Appendix. Measurements were taken at 5 (39°C) or 6 (33°C) conductivity values, corresponding to the solid curves. The vertical lines connect the experimental points (denoted by small circles) to the surface representing the best fit to all data.

3.2. ROT spectra

Typical spectra for 6m2 cells grown at 33 and 39°C are shown in Fig. 2. At the suspension conductivity of 56 mS/m, both cell types exhibited anti-field rotation at frequencies below ~ 3 MHz, while above this frequency co-field rotation occurred. The anti-field peak occurred at different frequencies for individual cells, spanning the range from 40 to 100 kHz for 6m2 cells grown at 33°C and

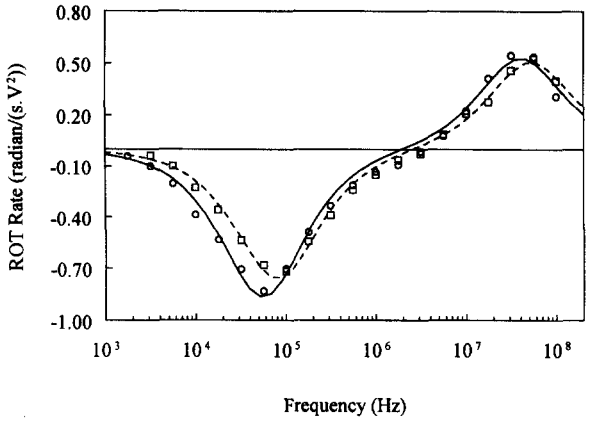

Fig. 2. Typical ROT spectra of 6m2 cells grown at 33°C (○, radius = 6.37 μm) and 39°C for 24 h (□, radius = 7.20 μm) suspended in a medium of conductivity 560 μS/cm. Each point is the average of four separate stopwatch measurements. Continuous curves show the best fit of the single-shell dielectric model. Parameters, with 90% confidence limits shown in parentheses, derived from the curve fits are as follows: 33°C cell, C_{mem} = 42.2 (39.2–45.2) mF/m², ϵ_{int} = 78.0 (67–89) and σ_{int} = 0.42 (0.37–0.47) S/m; 39°C cell, C_{mem} = 29.9 (28–31.8) mF/m², ϵ_{int} = 66.7 (55–78.4) and σ_{int} = 0.42 (0.38–0.46) S/m.

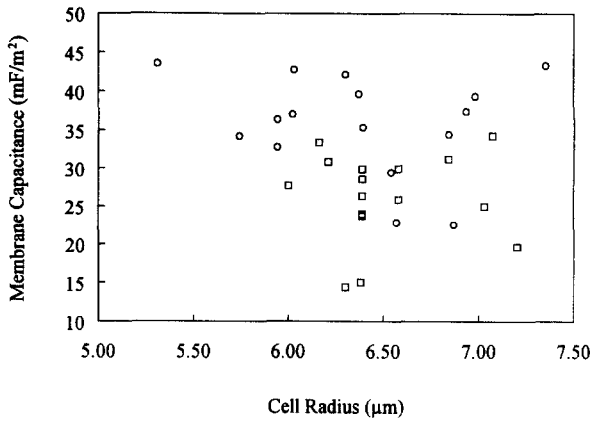

Fig. 3. The scatter plot of specific membrane capacitance, determined from electrorotation measurements, as a function of cell radius for individual 6m2 cells grown at 33°C (o) and 39°C for 24 h (□).

from 70 to 150 kHz for cells grown at 39°C, all for 24 h. The co-field peak occurred at a frequency of approx. 50 MHz for both cell types. The maximum cell rotation rate, which depended on the exact position of cells on the polynomial electrode, varied between 0.6 and 1.0 radian/(s · V²).

We have previously demonstrated [29] that only four dielectric parameters can be uniquely and accurately derived from an electrorotation spectrum consisting of two peaks. The simulation of ROT spectra using the single shell dielectric models involves five parameters, namely the specific membrane capacitance (C_{mem}) and conductance (G_{mem}), the cell internal conductivity (σ_{int}) and permittivity (ϵ_{int}), and a scaling factor related to the field strength and the viscosity of the ROT medium. In this work we have chosen to assume the membrane conductance is the same as that derived from the cDEP crossover frequency measurements and have then determined the other four parameters from the model. The means and standard deviations for each parameter are summarized in Table 1 for both 33°C and 39°C 6m2 samples.

The mean cell membrane specific capacitance values derived from the ROT spectra exhibited similar trends to those seen in the cDEP measurements, falling from 37.2 (±7.3) to 27.4 (±6.1) mF/m² when the cells were shifted from 33°C to 39°C for 24 h ($P < 0.001$). The mean cell interior conductivity and permittivity were found to be 0.49 (±0.07) S/m and 76.7 (±14.3), respectively, for cells grown at 33°C, and 0.51 (±0.06) S/m and 72.9 (±13.6) for cells shifted to 39°C for 24 h. However, these differences in the internal parameters were not statistically significant ($P > 0.1$). As observed previously for erythroleukemia DS19 cells [14], individual 6m2 cells under each treatment condition exhibited large variations for all dielectric parameters. For example, the specific membrane capacitance value of 6m2 cells grown at 33°C was found to range between 23.9 and 46.5 mF/m² for individual cells as evidenced by the scatter plot of the membrane capacitance as a function of cell radius shown in Fig. 3.

3.3. SEM studies

Fig. 4 shows scanning electron micrographs for 6m2 cells both grown in monolayer cultures on cover slips and

Table 1
Derived 6m2 cell dielectric parameters

	cDEP		ROT	
	33°C	39°C	33°C	39°C
Number of cells	344	106	17	16
r (μm)	6.23 (±0.69)	6.43 (±0.58)	6.49 (±0.69)	6.52 (±0.35)
C_{mem} (mF/m²)	42.3 (±1.3)	30.3 (±2.9)	37.2 (±7.3)	27.4 (±6.1)
G_{mem} (S/m²)	743 (±422)	567 (±326)	N/A	N/A
σ_{int} (S/m)	N/A	N/A	0.49 (±0.07)	0.51 (±0.06)
$\epsilon_{int}/\epsilon_o$	N/A	N/A	76.7 (±14.3)	72.9 (±13.6)

The parameters from cDEP measurements are given in the form of the averaged values and the confidence limits for a confidence level of 90%. The parameters from ROT spectra are given in the form of mean and standard deviation. The definitions of the symbols are as follows: r, cell radius; C_{mem} and G_{mem}: membrane-specific capacitance and conductance; σ_{int} and ϵ_{int}: cell interior conductivity and permittivity.

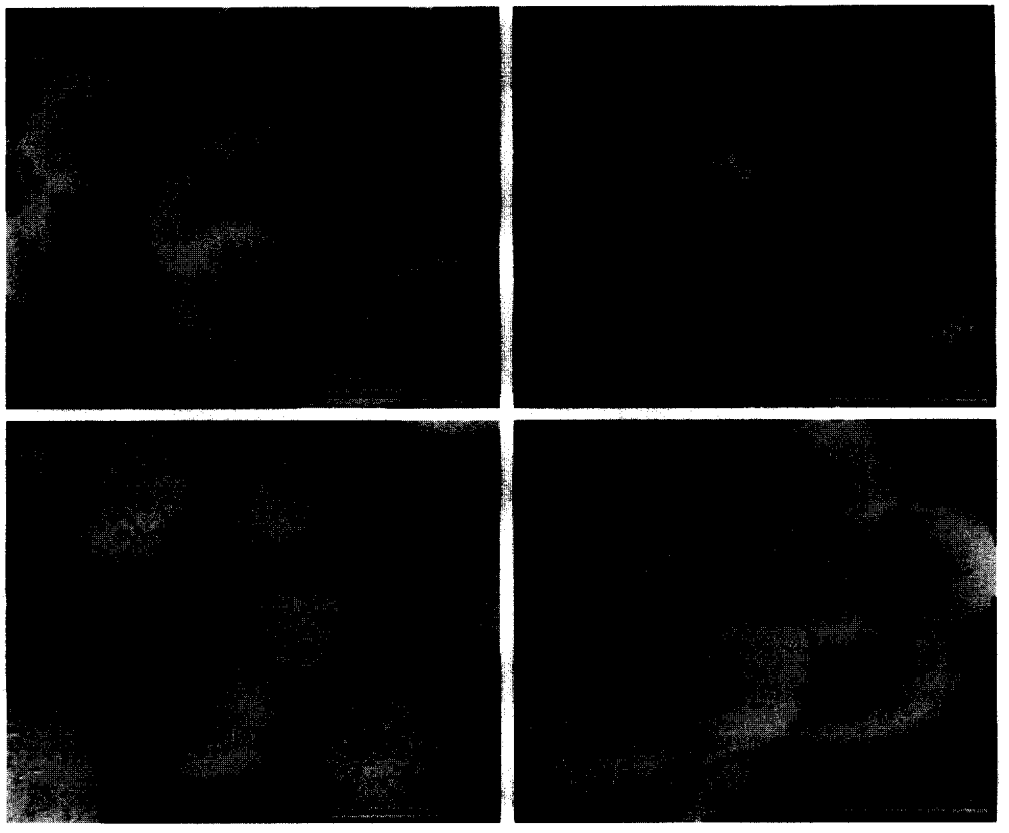

Fig. 4. Scanning electron micrographs of 6m2 cells. Monolayer culture: (A) cells grown at 33°C and (B) 24 h after shift to 39°C. Cells following harvest: (C) cells grown at 33°C and (D) 24 h after shift to 39°C. Bar length = 5 μm for (A–C) and 15 μm for (D).

in suspension following harvest. In agreement with a previous report for monolayer cultures [23], non-transformed 6m2 cells (39°C) exhibited a spread morphology with firm substrate attachment and a comparatively smooth surface, while transformed cells (33°C) had a more rounded appearance, a looser association with the substrate, and exhibited extensive microvilli on the plasma membrane surface. Cells resuspended after harvest also showed significantly different membrane morphologies. For the 6m2 cells at 33°C, cell surfaces were rich in microvilli of typical length ~ 1.5 μm and densities as high as 5–6 microvilli/μm^2. This contrasts with 39°C cells which exhibited a smoother, layered structural arrangement with far fewer microvilli on the surface and for which it was almost impossible to count the number of microvilli because of large smooth areas and bleb-like structures.

4. Discussion

Previously we reported ROT and cDEP measurements for the murine erythroleukemia cell line DS19 [10,12,14,17]. The focus was on changes in the dielectric properties that developed as these cells were induced to differentiate following treatment by hexamethylene bisacetamide (HMBA). Here we have extended our measurements to the rat kidney line 6m2, again as a function of induced cell differentiation. In this line, the transforming factor has been identified as the protein $P85^{gag\text{-}mos}$ resulting from a temperature-dependent splicing of oncogene products expressed by the cells following infection with the ts-110 mutant Moloney sarcoma virus [30]. When cultured at 33°C, the permissive temperature for $P85^{gag\text{-}mos}$ expression, 6m2 cells exhibit increased hexose transport [31], disarrayed microtubules and microfilaments [32], and other phenotypic alterations associated with transformation [23]. However, at 39°C, instability in the production of $P85^{gag\text{-}mos}$ results in the effective disappearance of this transforming protein from the cells and a concomitant change in phenotypic characteristics towards normalcy. We studied this 6m2 line because it not only represents an extension for us from cells that grow independently in suspension to those whose growth is attachment-dependent but also because it undergoes differentiation in response to a mild temperature treatment rather than through the use of a potentially membrane-interactive chemical agent. Furthermore, as described above, the molecular mechanisms underlying the 'retro-transformation' of 6m2 are known, allowing us, for the first time, to correlate dielectric changes in the cells with events relating to the expression of specific, identified genes.

4.1. Scatter plots

Measurements of both cDEP crossover frequencies and ROT spectra revealed significant differences between the electrokinetic responses of individual cells (Figs. 1 and 3). These differences were not correlated with the length of time cells were subjected to low ionic suspension, suggesting that the differences observed between the electrokinetic responses of individual 6m2 cells reflected true differences in their intrinsic dielectric characteristics. Such differences must in turn reflect significant heterogeneity in each cell population, possibly arising from factors including asynchrony of cells in their growth cycle [33], and differences in ploidy and size. Some heterogeneity can be predicted, for example, based on the simple concept that total cell volume and surface area must both be conserved when a cell divides into two equal daughter cells. In this case, prior to division, the mother cell must have at least a 26% excess of membrane if the two daughter cells are to be encompassed by an intact membrane. It follows that, even in the absence of other cell cycle-associated membrane alterations, the specific membrane capacitance should fall by 26% during cell division and then rise again by that amount as cells again cycle towards M-phase.

4.2. Membrane capacitance

We and others have analyzed [6,11,14] the physical factors that can influence the specific membrane capacitance, defined as the total membrane capacitance divided by the surface area of a smooth sphere whose radius is equal to that of the cell. The total capacitance is determined by the membrane dielectric permittivity (and hence its composition) as well as its thickness and area. We have estimated that the specific capacitance for a flat biological membrane of typical composition is ~ 9 mF/m^2 and concluded that the dominating factor underlying the large changes we have observed in membrane capacitance following manipulation cannot be accounted for by variations in this composition but instead reflect changes in the membrane surface configuration [11,14,24]. Membrane structures, such as microvilli, ruffles, folds and blebs increase the total membrane area and thus the total cell capacitance. Specific membrane capacitances are derived from the ROT and cDEP analyses using the single shell model assuming that the cells are smooth spheres and complex membrane structures therefore lead to the derivation of large specific capacitance values. Based on the SEM pictures of 6m2 cells, we estimated the average size and density of the microvilli on cell surfaces. For the cells at 33°C, cell surfaces contain as high as 5–6 microvilli/μm^2 with typical length ~ 1.5 μm and diameter 0.2 μm. Thus, membrane areas at 33°C (including the contributions from microvilli) can exceed those of smooth spheres of the same diameter by a factor of 5. This suggests that specific membrane capacitance values for 6m2 cells at 33°C based upon morphological arguments would range up to 45 mF/m^2, in good agreement with the values determined here from the single shell model analysis. On the other hand, 6m2 cells at 39°C exhibit a smoother membrane morphology, and hence should possess smaller membrane capacitances as observed (Fig. 3). Although there may be other, possibly unidentified, contributors to the differences between membrane specific capacitances of 6m2 cells at 33 and 39°C, we believe that it is the membrane structural configuration that is mainly responsible for this difference.

As indicated earlier, 6m2 cells synthesize an 85 kDa polyprotein (P85$^{gag\text{-}mos}$) [23,30,34,35] at 33°C that leads to their transformation. This protein disappears when the cells are maintained at 39°C on a time scale of several hours after the temperature shift [23,32,35]. Several physicochemical changes occur in the cells during this P85$^{gag\text{-}mos}$ disappearance phase, including an increase in transmembrane potential difference [21], a decrease in surface charge density [22] and the morphological alterations already described [23]. On a time scale of several days, the shift to 39°C results in significant changes in the microtubular system from being diffuse and poorly defined to being sharply-defined. In addition, F-actin cables alter from being sparse, short and poorly defined to being discrete, well developed and sharply defined. Since the observed changes in cell plasma membrane capacitance had already taken place when cells had been maintained to 39°C for 24 h and remained more or less constant thereafter (data not shown), they seem to correlate with the relatively short time scale alterations including those in membrane morphology, surface charge and transmembrane potential.

4.3. Membrane conductance

The cDEP crossover frequency measurements revealed that the membrane conductance for 6m2 cells fell from 743 ($\pm$422) to 567 ($\pm$326) S/m^2 following the shift from 33 to 39°C for 24 h. Due to the near-insulating nature of lipid bilayer, this observed membrane conductance mainly reflects the net transport of ionic species across the plasma membrane through pores, ion carriers, channels and pumps under the influence of the applied electric field. Ionic conductance through membrane pores is considered to reflect their density and size. However, quantifying such a conductance contribution without knowledge of the nature of the membrane pores present on the 6m2 cells is difficult, and to complicate matters further, it is not clear whether the brief trypsinization used during the harvesting of cells would have affected their membrane integrity or pores. Nevertheless, the observed drop in specific membrane conductance when 6m2 cells were shifted to 39°C was in direct proportion to the changes in specific capacitance already discussed. Applying the same cell surface area considerations, the observed conductance change may also be accounted for by the reduction of total membrane

surface area of the 6m2 cells if it is assumed that the conductance of the perfectly smooth membrane remain unchanged at 186 S/m^2.

Although the membrane conductance of 6m2 cells due to ionic channels is currently not known, values below 100 S/m^2 have been reported as typical for many mammalian cell types [36]. If we assume that 6m2 cells also behave in this way, then we can conclude that ion channels alone cannot account for the observed larger membrane conductance values. Another source for the measured membrane conductance is the component of surface conductivity parallel to the membrane surface due to the counter ion layer induced at negatively-charged cell surfaces sites [37]. This contribution to membrane conductance due to surface conduction can be estimated as being < 50 S/m^2 [6,37].

Finally, we note that while the total membrane conductance values derived here from cDEP measurements are more than three times larger than those (typically less than 200 S/m^2) measured by ROT for several other mammalian cell types in suspensions of much lower conductivity [6,11,12], our measured values closely approximate those found for murine myeloma cells [7] measured under experimental conditions similar to our own.

4.4. Internal dielectric parameters

We recently reported measurements of the internal dielectric properties of DS19 cells determined by ROT measurements [38] and for those cells the mean cell interior relative permittivity was found to exceed the value for pure water by 12. We showed further that neither the cell nucleus, nor mitochondria, nor biomolecules in the cytoplasm could account for such a large internal permittivity increment. Here, however, the mean cell interior relative permittivities for the 6m2 cells at 33 and 39°C were found to be ~ 73 and ~ 77, respectively, larger than those determined previously for other cell types with dielectric impedance measurement on cell suspensions (e.g., Ref. [39]). As demonstrated in our discussion concerning the dielectric properties of DS19 cells [38], these values for 6m2 cells can be readily rationalized by taking into account that we used a single-shell dielectric model to analyze the 'three-shell' cells consisting of both nuclear and plasma membranes. The internal electrical conductivities found here for 6m2 cells are smaller than those observed previously for DS19 cells [38]. This is probably accounted for by the larger ionic leakage through the plasma membrane of the 6m2 cells as reflected by their larger membrane conductance values.

4.5. Viral transformation

Our earlier results for DS19 and HL-60 cells and those reported here for 6m2 cells span two classes of mammalian cells, namely those whose growth is attachment-independent (the blood-derived cells DS 19 and HL-60 that grow in suspension) or attachment-dependent (the kidney-derived cells 6m2 that grow in monolayers). On the other hand, both DS19 and 6m2 cells owe their transformation state to viral agents and the possibility that viral involvement also occurred in the transformation of HL-60 cells cannot be ruled out. It follows that while the cell types examined in our studies are distinct, the mechanisms of transformation may be similar. In all cases, the transformed phenotype is characterized by an increased morphological complexity of the cell membrane surface and a correspondingly larger specific membrane capacitance and conductance. It will be of great interest to determine whether such changes are specific to viral transformation or whether they are general to the malignant state.

4.6. Parallels between membrane dielectric and surface charge responses to differentiation

In addition to the dielectric changes reported here for 6m2 cells, it has been shown previously that the specific surface charge density, as determined by cellular electrophoresis, falls when 6m2 [22] cells, as well as the DS19 [40] and HL-60 (unreported findings) lines, are induced to differentiate. These changes in effective cell surface net charge have been related to alterations in the sialic acid content of the glycocalyx [41] of the differentiating cells. While the basis for the dielectric changes reported here and for such surface charge modifications might at first sight appear unrelated, we note that these two responses can, in fact, be rationalized in terms of the same underlying mechanism. This is because a change in effective membrane surface charge density could result not only from an alteration in the number of sialic acid residues per unit area of cell membrane but also from a change in the total area of membrane that covers a cell, just as in the case of the cell specific membrane capacitance. Thus we note that the drop in surface charge density following a shift from 33 to 39°C was from -18.5 to -14.2 mC/m^2, a decrease of 23%, for 6m2 cells [22]. This corresponds closely to the drop observed here in specific capacitance, a decrement of 26%. If it is assumed that the charge per unit area of smooth membrane actually remained constant at -4.7 mC/m^2 when 6m2 cells changed their phenotype while the total area of membrane covering the cells fell by 23%, then the surface charge and dielectric data are in complete agreement. Such a 'fixed' charge density on 6m2 cells corresponds to a mean spacing of charged sialic acid residues of 34 nm on a smooth membrane surface.

Similar agreement is found for DS19 cells following treatment with the differentiating agent hexamethylene bisacetamide. In that case cell surface membrane capacitance dropped from 17.4 to 15.3 mF/m^2 (a reduction of 12%) [14] and cell electrophoretic mobility fell from -1.01×10^{-8} to -0.88×10^{-8} $m^2/(V.s)$ (a drop of 13%) [39]. In that case, and using arguments from [22] relating the cell electrophoretic mobility (EPM) to the

surface charge density, we derive an effective 'fixed' charge per unit area of smooth DS19 membrane of -5.2 mC/m^2, very close to the value found above for smooth 6m2 membrane. It follows that the surface charge and dielectric responses of 6m2 and DS19 cells to differentiation treatment are both completely consistent with a membrane morphological interpretation.

We note that many attempts have been made to correlate EPM with cellular transformation and malignancy [42] as well as with cell activation [43]. Based on the above arguments, we believe it is possible that the changes previously reported in EPM in those experiments may in many cases have reflected alterations in cell surface conformation rather than true modifications of the sialic acid density on the smooth membranes.

Acknowledgements

We are grateful to James Syrewicz for culturing the 6m2 cells used in this study, to Kim Dulski for SEM work, and to Dr. Edwin Murphy, Jr. for helpful discussions. This work was supported in part by the National Foundation for Cancer Research and the Sid W. Richardson Foundation. Electron microscopy was made possible by NIH Core Grant P30-CA16672.

Appendix A. cDEP crossover analysis

The cDEP crossover frequency is a function of the dielectric properties of a particle and its suspending medium, given by Ref. [44]

$$f_{cross} = \frac{1}{2\pi}\left(\frac{(2\sigma_m + \sigma_p)(\sigma_m - \sigma_p)}{(2\epsilon_m + \epsilon_p)(\epsilon_p - \epsilon_m)}\right)^{1/2} \quad (A.1)$$

where ϵ_i and σ_i are the dielectric permittivity and electrical conductivity, respectively, for the particle (i = p) or medium (i = m). For a biological cell, the interfacial polarization between the plasma membrane and the cytoplasm results in a dispersion typically around 1 MHz for the cell effective dielectric permittivity and electrical conductivity. For frequency range well below the dispersion frequency, the cell dielectric properties can be shown to be related to the membrane properties by the simple proportionalities

$$\epsilon_{pDC} \approx r\epsilon_{mem}/d, \quad (A.2)$$

and

$$\sigma_{pDC} \approx r\sigma_{mem}/d. \quad (A.3)$$

For a typical cell radius of 5 μm for 6m2 cells encountered here, the parameter ϵ_{pDC} is of the order of 2200 ϵ_o ($\epsilon_{mem} = 2.2\epsilon_o$). Thus, Eq. (A.1) can be approximated in terms of the specific membrane capacitance ($C_{mem} = \epsilon_{mem}/d$) and conductance ($G_{mem} = \sigma_{mem}/d$),

$$f_{cross} = \frac{\sqrt{2}}{8\pi r C_{mem}}\sqrt{(4\sigma_m - rG_{mem})^2 - 9r^2G_{mem}^2}. \quad (A.4)$$

We constructed an optimization algorithm to determine C_{mem} and G_{mem} by adjusting the model parameters so as to minimize the error between the measured and theoretically-determined crossover frequencies

$$\underset{G_{mem}C_{mem}}{Min} \sum_i (f_{cross\_theory i} - f_{cross\_exp.i})^2, \quad (A.5)$$

where i corresponds to each experimental point, and f_{cross_theory} is calculated using Eq. (A.4). A non-linear contour method [45] was then used to estimate the confidence limits for C_{mem} and G_{mem}.

It is worthwhile to note that the C_{mem} and G_{mem} are flat surface approximations to the properties of a 3-dimensional structure (the membrane-plus-microvilli), and these parameters, as well as the dielectric permittivity (ϵ_{int}) and electrical conductivity (σ_{int}) of cell interior are assumed to be frequency-independent over the whole frequency range investigated in the study. Several factors may affect the validity and accuracy of Eq. (A.4) for determining crossover frequencies. Eq. (A.2) and Eq. (A.3) require that the cell intrinsic Maxwell interfacial polarization occurs at a frequency much higher than the observed crossover frequency and that the cell internal conductivity be much higher than that of the plasma membrane. For the 6m2 cells examined here, the minimum interfacial polarization frequency, as calculated from the derived dielectric parameters (with their variations taken into account), was about 500 kHz and the derived internal conductivity was above 0.2 S/m, fully three orders of magnitude larger than the conductivity of the plasma membrane. These factors indicate that the effective dielectric permittivity and conductivity in the crossover frequency range observed here were derived with very good accuracy using Eq. (A.4).

A possible complication of mammalian cell measurements is ionic leakage from the cytoplasm into suspension medium under low ionic strength conditions [10]. For all the experiments performed in this work, cells were typically suspended at a concentration of 3×10^6/ml and less than 1% change in D.C. conductivity of the suspensions was detected over a time period of $\sim$ 30 min. It follows that this possible problem did not prove to be a difficulty in the case of 6m2 cells.

References

[1] Arnold, W.M., Geier, B.M., Wendt, B. and Zimmermann, U. (1986) Biochim. Biophys. Acta 889, 35–48.
[2] Ziervogel, H., Glaser, R., Schadow, D. and Heymann, S. (1986) Biosci. Rep. 6, 973–982.
[3] Fuhr, G., Muller, T., Hagedorn, R. and Torner, H. (1987) Biochim. Biophys. Acta 930, 65–71.

[4] Arnold, W.M., Schmutzler, R.K., Al-Hasani, S., Krebs, D. and Zimmermann, U. (1989) Biochim. Biophys. Acta 979, 142–146.
[5] Fuhr, G., Rosch, P., Muller, T., Dressler, V. and Goring, H. (1990) Plant Cell Physiol. 31, 975–985.
[6] Hu, X., Arnold, W.M. and Zimmermann, U. (1990) Biochim. Biophys. Acta 1021, 191–200.
[7] Gimsa, J., Marszalek, P., Loewe, U. and Tsong, T.Y. (1991) Biophys. J. 60, 749–760.
[8] Hölzel, R. and Lamprecht, I. (1992) Biochim. Biophys. Acta 1104, 195–200.
[9] Huang, Y., Hölzel, R., Pethig, R. and Wang, X-B. (1992) Phys. Med. Biol. 37, 1499–1517.
[10] Gascoyne, P.R.C., Pethig, R., Burt, J.P.H. and Becker, F.F. (1993) Biochim. Biophys. Acta 1149, 119–126.
[11] Sukhorukov, V.L., Arnold, W.M. and Zimmermann, U. (1993) J. Membr. Biol. 132, 27–40.
[12] Gascoyne, P.R.C., Noshari, J., Becker, F.F. and Pethig, R. (1994) IEEE. Trans. Ind. Appl. 30, 829–834.
[13] Gimsa, J., Schnelle, Th., Zechel, G. and Glaser, R. (1994) Biophys. J. 66, 1244–1253.
[14] Wang, X-B., Huang, Y., Gascoyne, P.R.C., Becker, F.F., Hölzel, R. and Pethig, R. (1994) Biochim. Biophys. Acta 1193, 330–344.
[15] Becker, F.F., Wang, X-B., Huang, Y., Pethig, R., Vykoukal, J. and Pethig, R. (1995) Proc. Natl. Acad. Sci. 92, 860–864 (USA).
[16] Egger, M. and Donath, E. (1995) Biophys. J. 68, 364–372.
[17] Gascoyne, P.R.C., Huang, Y., Pethig, R., Vykoukal, J. and Becker, F.F. (1992) Meas. Sci. Technol. 3, 439–445.
[18] Wang, X-B., Huang, Y., Burt, JP.H., Markx G.H. and Pethig, R. (1992) J. Phys. D: Appl. Phys. 26, 1278–1285.
[19] Becker, F.F., Wang, X-B., Huang, Y., Pethig, R., Vykoukal, J. and Pethig, R. (1994) J. Phys. D: Appl. Phys. 27, 2659–2662.
[20] Markx, G., Huang, Y., Zhou, X.F. and Pethig, R. (1994) Microbiology 140, 585–591.
[21] Lai, C.N., Gallick, G.E., Arlinghaus, R.B. and Becker, F.F. (1984) J. Cell. Physiol. 121, 139–142.
[22] Price, J.A.R., Pethig, R., Lai, C.-N., Becker, F.F., Gascoyne, P.R.C. and Szent-Györgyi, A. (1987) Biochim. Biophys. Acta 989, 129–136.
[23] Lai, C-N., Gallick, G.F., Maxwell, S.A., Brinkley, B.R. and Becker, F.F. (1988) J. Cell. Physiol. 134, 445–452.
[24] Arnold, W.M., Klarmann B.G., Sukhorukov V.L. and Zimmermann U. (1992) Biochem. Soc. Trans. 20, 120S.
[25] Blair, D.G., Hull, M.A. and Finch, E.A. (1979) Viorology 95, 303–316.
[26] Nash, M.A., Brizzard, B.L., Wong, J.L. and Murphy Jr., E.C. (1985) J. Virol. 53, 624–633.
[27] Huang, Y. and Pethig, R. (1991) Meas. Sci. Technol. 2, 1142–1146.
[28] Hughes, M.P., Wang, X-B., Becker, F.F., Gascoyne, P.R.C. and Pethig, R. (1994) J. Phys. D: Appl. Phys. 27, 1564–1570.
[29] Gascoyne, P.R.C., Becker, F.F. and Wang, X-B. (1995) Bioelectrochem. Bioenerg. 36, 115–125.
[30] Stanker, L.H., Gallick, G.E., Horn, J.P. and Arlinghaus, R.B. (1983) J. Gen. Virol. 64, 2203–2211.
[31] Horn, J.P., Wood, T.G., Blair, D.G. and Arlinghaus, R.B. (1980) Virology 105, 516–525.
[32] Brown, R.L., Horn, J.P., Wible, L., Arlinghaus, R.B. and Brinkley, B.R. (1981) Proc. Natl. Acad. Sci. USA 78, 5593–5597.
[33] Sukhorukov V.L., Djuzenova C.S., Arnold W.M. and Zimmermann U. (1994) J. Membrane Biol. 142, 77–92.
[34] Gallick, G.E., Hamelin, R., Maxwell, S., Duyka, D. and Arlinghaus, R.B. (1984) Virology 139, 366–374.
[35] Maxwell, S.A. and Arlinghaus, R.B. (1985) J. Gen. Viorl. 66, 2135–2146.
[36] Lewis, S.A. and Hanrahan, J.W. (1986) in New Insights into Cells and Membrane Transport Processes (Poste, G. and Crooke, S.T., Eds.), Plenum Press, New York, pp. 305–326.
[37] Arnold, W.M., Schwan, H.P. and Zimmermann, U. (1987) J. Phys. Chem. 91, 5093–5098.
[38] Huang, Y., Wang, X-B., Becker, F.F. and Gascoyne, P.R.C. (1995) Phys. Med. Biol. 40, 1789–1806.
[39] Asami K., Takahashi Y. and Takashima S. (1989) Biochim. Biophy. Acta 1010, 49–55.
[40] Gascoyne, P.R.C. and Becker, F.F. (1990) J. Cell Physiol. 142, 309–315.
[41] Shimizu, M. and Iwaguchi, T. (1987) Electrophoresis 8, 556–559.
[42] Lowick, J.H.B., Purdom, L., James, A.M. and Ambrose, E.J. (1961) J. Roy. Med. Soc. 80, 47–57.
[43] Bauer, J. and Hannig, K. (1985) Electrophoresis 6, 301–306.
[44] Jones, T.B. and Kallio, G. A. (1979) J. Electrostat. 6, 207–224.
[45] Draper, N.R. and Smith, H. (1980) Applied Regression Analysis Chap. 10, pp. 472–485, Wiley, New York.